scientific reports

Check for updates

OPEN

# Drastic improvement of Curie temperature by chemical pressure in *N*-type diluted magnetic semiconductor $Ba(Zn,Co)_2As_2$

Licheng Fu[1], Yilun Gu[1], Guoxiang Zhi[1], Haojie Zhang[1], Rufei Zhang[1], Jinou Dong[1], Xueqin Zhao[1], Lingfeng Xie[1] & Fanlong Ning[1,2]✉

**We report the effect of chemical pressure on the ferromagnetic ordering of the recently reported *n*-type diluted magnetic semiconductor $Ba(Zn_{1-x}Co_x)_2As_2$ which has a maximum $T_C \sim 45$ K. Doping Sb into As-site and Sr into Ba-site induces negative and positive chemical pressure, respectively. While conserving the tetragonal crystal structure and *n*-type carriers, the unit cell volume shrink by ~ 0.3% with 15% Sr doping, but drastically increase the ferromagnetic transition temperature by 18% to 53 K. Our experiment unequivocally demonstrate that the parameters of $Zn(Co)As_4$ tetrahedra play a vital role in the formation of ferromagnetic ordering in the $Ba(Zn,Co)_2As_2$ DMS.**

Diluted magnetic semiconductors (DMSs) that combine the properties of semiconductors and ferromagnets are promising materials for spintronic devices owing to the possible manipulation of both spin and charge degrees of freedom[1–4]. In 1990s, based on the non-equilibrium growth conditions of low temperature Molecular Beam Epitaxy (LT-MBE) method, some DMSs thin films, such as (Ga,Mn)As and (In,Mn)As, were successfully prepared and show hole-induced ferromagnetic ordering[5,6]. Among them, (Ga,Mn)As is one of many well investigated DMSs and it has been realized many spintronic functionalities in the last three decades[7–9]. In (Ga,Mn)As, spins and holes are introduced by $Mn^{2+}/Ga^{3+}$ substitutions simultaneously. The highest $T_C$ obtained in (Ga,Mn)As is ~ 200 K when $Mn^{2+}$ doping level reaches ~ 12%[10], which is still below room temperature that are required for practical applications. On the other hand, high temperature ferromagnetism with *n*-type carriers has been reported in Fe-doped (In,Fe)As and (In,Fe)Sb films, the Fe atoms play the role of local magnetic moments, while free carriers are induced separately by codoped nonmagnetic donors/acceptors or native defects[11–13].

In recent years, some new series of bulk form DMSs, that are iso-structure to the iron-based superconductors were reported. Such as 111-type Li(Zn,Mn)As[14], Li(Zn,Mn)P[15], 1111-type (La,Ba)(Zn,Mn)AsO[16] and 122-type $(Ba,K)(Zn,Mn)_2As_2$[17,18], which are iso-structure to the iron-based superconductors LiFeAs[19], $LaFeAsO_{1-\delta}$[20] and $(Ba,K)Fe_2As_2$[21], respectively. In these new materials, spins and carriers are introduced at different ionic sites, which makes it possible to manipulate them separately, and investigate their unique contributions to the ferromagnetic ordering. In addition, the bulk form samples enable the utilization of some experimental techniques such as neutron scattering, nuclear magnetic resonance (NMR) and muon spin relaxation ($\mu SR$) that are usually based on bulk form materials[14–17,22–24].

Among these new bulk form DMSs, the Curie temperature of $(Ba,K)(Zn,Mn)_2As_2$ has reached as high as ~ 230 K[18]. This temperature is still below room temperature requested for practical applications. For the purpose of improving $T_C$, both physical pressure and chemical pressure effects on $(Ba,K)(Zn,Mn)_2As_2$ have been studied[25–27]. Unexpectedly, the results show that the Curie temperature is suppressed by both external physical pressure and chemical pressure. Recently, our group reported the successful synthesis of a new *n*-type DMS $Ba(Zn_{1-x}Co_x)_2As_2$[28] iso-structure to the *p*-type $(Ba,K)(Zn,Mn)_2As_2$. The $T_C$ reaches ~ 45 K for $x = 0.04$. $\mu SR$ measurements have confirmed that the ferromagnetic ordering in $Ba(Zn,Co)_2As_2$ is homogeneous and intrinsic. We wonder how lattice expansion or reduction will affect the ferromagnetism in $Ba(Zn,Co)_2As_2$ and what parameters affect the ferromagnetic ordering the most.

In this paper, we report the chemical pressure effect of Sr substitution for Ba and Sb substitution for As on the *n*-type DMS $Ba(Zn_{0.96}Co_{0.04})_2As_2$ with $T_C \sim 45$ K. We introduce positive and negative chemical pressure

[1]Zhejiang Province Key Laboratory of Quantum Technology and Device and Department of Physics, Zhejiang University, Hangzhou 310027, China. [2]Collaborative Innovation Center of Advanced Microstructures, Nanjing University, Nanjing 210093, China. ✉email: ningfl@zju.edu.cn

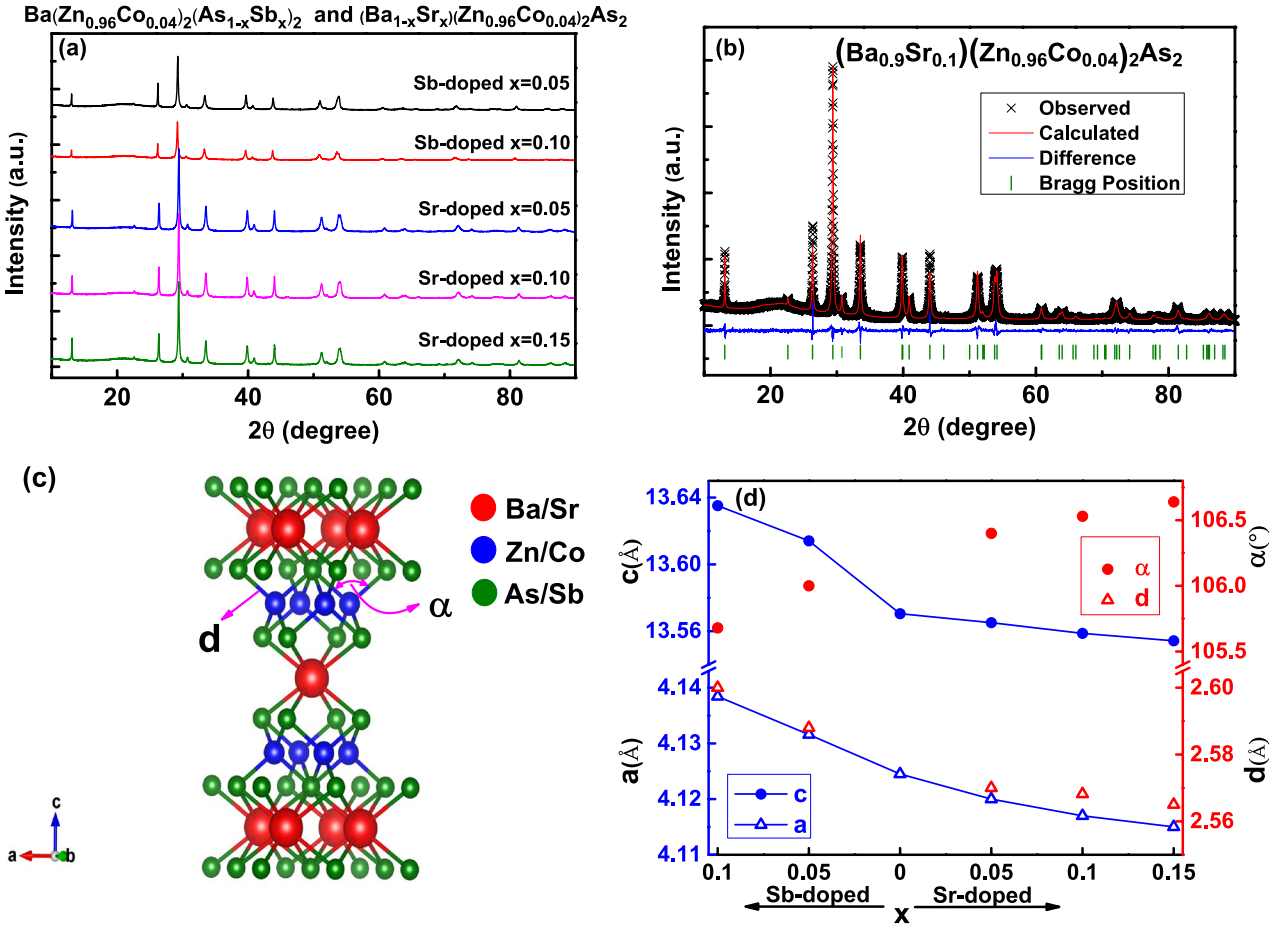


**Figure 1.** (**a**) The X-ray diffraction patterns for polycrystalline Sr-doped $(Ba_{1-x}Sr_x)(Zn_{0.96}Co_{0.04})_2As_2$ ($x$ = 0.05, 0.10 and 0.15) and Sb-doped $Ba(Zn_{0.96}Co_{0.04})_2(As_{1-x}Sb_x)_2$ ($x$ = 0.05 and 0.10). (**b**) The Rietveld refinement of $(Ba_{0.9}Sr_{0.1})(Zn_{0.96}Co_{0.04})_2As_2$. (**c**) The crystal structure of $BaZn_2As_2$ with tetragonal phase. The average As/Sb-Zn/Co band length is marked as $d$ and the average As/Sb-Zn/Co-As/Sb bond angle is marked as $\alpha$ (bisected by $c$ axis). (**d**) The lattice parameters, bond length $d$ and bond angle $\alpha$ obtained from the Rietveld refinements for both Sb-doped and Sr-doped samples. The lattice parameters of $Ba(Zn_{0.96}Co_{0.04})_2As_2$ are extracted from Fig. 1c of ref.[28].

through Sr/Ba and Sb/As iso-valent substitution, respectively, to study the chemical pressure effect on the ferromagnetic ordering in $Ba(Zn,Co)_2As_2$. We find that 15% Sr substitution for Ba drastically improve $T_C$ by 18% to 53 K while conserving the tetragonal structure and $n$-type carriers. Our experiment unequivocally demonstrate that the parameters of $Zn(Co)As_4$ tetrahedra play a vital role in the formation of ferromagnetic ordering in the $Ba(Zn,Co)_2As_2$ DMS.

## Results and discussion

**X-ray diffraction.** In Fig. 1a, we show polycrystalline X-ray diffraction patterns of Sr-doped $(Ba_{1-x}Sr_x)(Zn_{0.96}Co_{0.04})_2As_2$ ($x$ = 0.05, 0.10 and 0.15) and Sb-doped $Ba(Zn_{0.96}Co_{0.04})_2(As_{1-x}Sb_x)_2$ ($x$ = 0.05 and 0.10). We should mention that $BaZn_2As_2$ exhibit two different crystal structures, the low-temperature orthorhombic phase $\alpha$ -$BaZn_2As_2$ (space group Pnma)[29] and the high-temperature tetragonal phase $\beta$-$BaZn_2As_2$ (space group I4/mmm) as a semiconductor with a bandgap ~ 0.2 eV[30,31]. Both $p$-type DMS $(Ba,K)(Zn,Mn)_2As_2$ and $n$-type DMS $Ba(Zn,Co)_2As_2$ were achieved in the high temperature tetragonal phase[17,28]. The X-ray diffraction patterns for all samples can be well indexed by the tetragonal $\beta$-$BaZn_2As_2$ phase, and no orthorhombic $\alpha$-$BaZn_2As_2$ phase exist. That is, neither positive nor negative chemical pressure change the tetragonal crystal structure. In Fig. 1b, as an example, we show the Rietveld refinement of $(Ba_{0.9}Sr_{0.1})(Zn_{0.96}Co_{0.04})_2As_2$ with tetragonal $\beta$ -$BaZn_2As_2$ phase using an open-source package GSAS-II[32]. The resultant weighted reliable factor $R_{wp}$ is ~ 7.9 %. The crystal structure of the tetragonal phase is shown in Fig. 1c, which can be viewed as [ZnAs] layers(consist of $ZnAs_4$ tetrahedra) stacking alternately with Ba layers along the $c$ axis. In Fig. 1d, we show the lattice parameters, the averaged $(As_{1-x}Sb_x)$-$(Zn_{0.96}Co_{0.04})$ band length $d$ and the averaged $(As_{1-x}Sb_x)$-$(Zn_{0.96}Co_{0.04})$-$(As_{1-x}Sb_x)$ bond angle $\alpha$ obtained from the Rietveld refinements for different doping levels. We can see that for Sb-doped samples, lattice parameters $a$, $c$ and bond length $d$ increase monotonically with the increasing of doping levels; This is because the atomic radius of As and Sb are 1.25 Å and 1.33 Å, respectively. Substitution of Sb for As

therefore produce a negative chemical pressure. On the other hand, the ionic radius of $Ba^{2+}$ and $Sr^{2+}$ are 1.35 Å and 1.13 Å, respectively. Therefore, substitution of Sr for Ba decrease $a$, $c$ and the bond length $d$, which produce positive chemical pressure. For a non-distorted ideal tetrahedron, bond angle should be 109.47°. In our samples, with more Sb doping, $\alpha$ tends to deviate from the ideal value; while with more Sr doping, the $\alpha$ tends to be more close to the value of 109.47°.

**Magnetic properties.** In Fig. 2a, we show the temperature dependent magnetization for both Sb-doped and Sr-doped samples in zero-field cooling (ZFC) and field cooling (FC) conditions with an applied external field of 100 Oe. No significant magnetic transition are observed above 60 K. Abrupt increase of magnetization takes place at lower temperature, indicating the ferromagnetic transition. Compared to the $Ba(Zn_{0.96}Co_{0.04})_2As_2$ whose $T_C$ is 45 K, we can see that the transition moves to lower temperature region with Sb doping while moves to higher temperature region with Sr doping. This trend can also be seen in the plot of $dM(T)/dT$ versus $T$, as shown in Fig. 2b. The minimum value of $dM/dT$ decreases with Sb doping, and increases with Sr doping. In Fig. 2c, we show the isothermal magnetization curves for both Sb-doped and Sr-doped samples at 2 K. Clear hysteresis loops demonstrate the ferromagnetic ordering state with the coercive field $\sim$ 10 Oe, which is similar to the $Ba(Zn_{0.96}Co_{0.04})_2As_2$[28].

We fit the paramagnetic part of the temperature dependent magnetization curves with a modified Curie-Weiss formula, $(\chi - \chi_0)^{-1} = (T - \theta)/c$, $\chi_0$ is a temperature-independent component, $C$ is the Curie constant and $\theta$ is the Weiss temperature. In Fig. 2d, we show the $(\chi - \chi_0)^{-1}$ versus temperature plots with temperature range from 100 to 200 K, much higher than the ferromagnetic transition temperature. Through linear-fitting, we can get Weiss temperature $\theta$ from the intersection of the linear-fit lines and $x$ axis. The effective moment $\mu_{eff}$ can also be obtained by using formula $C = N\mu_0\mu_{eff}^2/3K_B$. Furthermore, to determine the Curie temperature ($T_C$) accurately, Arrot-Noakes plots[33,34] (through redraw the iso-thermal magnetization curves as $M^2$ versus $H/M$) were applied to the Sr-doped samples. Around $T_C$, the data points should form a series of parallel lines in the high field region; while at $T_C$, the parallel line should pass through the origin. In Fig. 2e, we show the Arrot-Noakes plots and the linear-fitting in high field region for $(Ba_{0.9}Sr_{0.1})(Zn_{0.96}Co_{0.04})_2As_2$, the $T_C$ is identified as 52 K.

In Table 1, we list all these parameters obtained above. Comparing with those of $Ba(Zn_{0.96}Co_{0.04})_2As_2$[28], we can see that the $T_C$ decreases with negative chemical pressure induced by Sb-doping, similar behavior has also been observed in Sb-doped $p$-type $(Ba,K)(Zn,Mn)_2As_2$[25]. While for Sr-doped samples, which provide positive chemical pressure, $T_C$ moves to the high temperature region. This is opposite to the case observed in $(Ba,K)(Zn,Mn)_2As_2$, where positive chemical pressure induced by P/As substitution suppress the $T_C$[25]. Previous results have shown that long-range ferromagnetic interaction in many $p$-type DMSs is predominantly mediated by the itinerant carries[26,27,35–39]. In $p$-type $(Ba,K)(Zn,Mn)_2As_2$, the long-range magnetic ordering is mediated by the $p$ states of As through As 4$p$-Mn 3$d$ hybridization. Shortened Zn/Mn-As bond length and optimized As-Zn/Mn-As bond angle (109.47° for an ideal tetrahedron) will enhance this $p$-$d$ hybridization and the indirect exchange interaction between Mn dopants. Applying physical pressure to $(Ba,K)(Zn,Mn)_2As_2$ will decrease Zn/Mn-As bond length and drive the As-Zn/Mn-As bond angle away from 109.47°. Therefore, $T_C$ is suppressed[27]. In $n$-type $Ba(Zn,Co)_2As_2$, with the same crystal structure, as shown in Fig. 1d, the bond length $d$ increases and the bond angle $\alpha$ deviates from the ideal value with Sb-doping. While for Sr-doped samples, instead of the direct influence on the $Zn(Co)As_4$ tetrahedra with substitution on As sites, the Sr/Ba substitution manipulates the lattice parameters and then moderately shortens the bond length $d$ and drive the bond angle $\alpha$ close to the ideal value of 109.47°. We conclude that the parameters of $Zn(Co)As_4$ tetrahedra plays an important role in the formation of ferromagnetic ordering in $n$-type $Ba(Zn,Co)_2As_2$ DMS, the more $(As_{1-x}Sb_x)$-$(Zn_{0.96}Co_{0.04})$-$(As_{1-x}Sb_x)$ bond angle $\alpha$ closer to 109.47°, the higher Curie temperature can be achieved.

**Transport and Hall effect.** In Fig. 3a, we show the temperature-dependent resistivity of Sr-doped and Sb-doped $Ba(Zn_{0.96}Co_{0.04})_2As_2$ samples, respectively. For all studied samples, the resistivity increases with decreasing temperature, indicating that our samples retain semiconducting behavior under either positive or negative chemical pressure. For Sb-doped sample, the resistivity quickly increases with decreasing temperature and is much higher than that of $Ba(Zn_{0.96}Co_{0.04})_2As_2$ in low temperature region. While in contrast, the resistivity of Sr-doped sample is lower than that of $Ba(Zn_{0.96}Co_{0.04})_2As_2$ in most temperature range. This can be attribute to the broadened electronic bandwidth and increased carrier mobility with compression of the lattice[26,35]. To examine whether the type of carriers for Sr-doped samples with iso-valent doping has been changed, we measured Hall effect. We show $(Ba_{0.9}Sr_{0.1})(Zn_{0.96}Co_{0.04})_2As_2$ as an example in Fig. 3b. The negative slope of the Hall resistivity at different temperatures demonstrates that the dominant carriers are electrons and the carrier concentration is roughly estimated to be $\sim 10^{18}/cm^{-3}$, comparable to $Ba(Zn_{0.96}Co_{0.04})_2As_2$[28]. These results demonstrate that positive chemical pressure induced by Sr/Ba substitution increases the ferromagnetic transition temperature $T_C$ and electrons are still dominant carriers.

## Conclusion

To conclude, we have successfully synthesized both Sr-doped $(Ba_{1-x}Sr_x)(Zn_{0.96}Co_{0.04})_2As_2$ and Sb-doped $Ba(Zn_{0.96}Co_{0.04})_2(As_{1-x}Sb_x)_2$ DMSs via solid-state reaction method. The X-ray diffraction measurements confirm that both Sr-doped and Sb-doped samples retain the tetragonal crystal structure. Hall effect measurements show that the dominant carriers are still electrons for Sr-doped sample. Magnetization measurements reveal that the ferromagnetic transition temperature $T_C$ decreases with Sb-doping while increases by 18% to 53 K with 15% Sr-doping. Comparing with the results of $p$-type $(Ba,K)(Zn,Mn)_2As_2$[25,27], we find that the parameters of $Zn(Co)As_4$ tetrahedra have great influence on the formation of ferromagnetic ordering. Our work shows an effective method to modify the magnetic properties of $n$-type DMS $Ba(Zn,Co)_2As_2$ via proper chemical pressure and

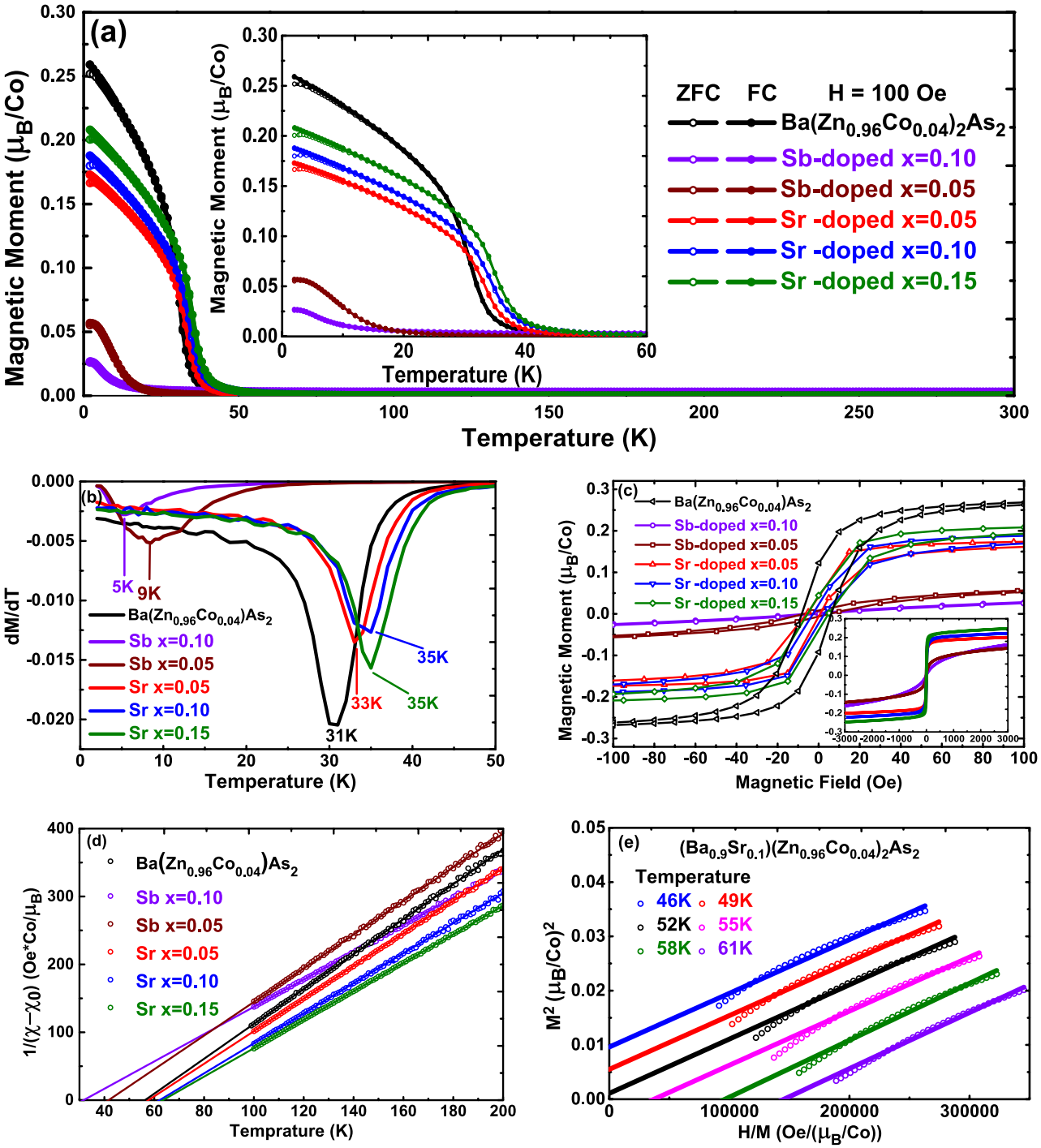


**Figure 2.** (**a**) Temperature dependent magnetization for Sb-doped and Sr-doped samples in zero-field cooling (ZFC) and field cooling (FC) conditions with an applied external field of 100 Oe. Inset shows the partial enlarged curves with temperature from 2 to 60 K. The M-T data of $Ba(Zn_{0.96}Co_{0.04})_2As_2$ extracted from Fig. 3a of ref.[28]; (**b**) The $dM(T)/dT$ versus $T$ curves. (**c**) The isothermal magnetization curves for both Sb-doped and Sr-doped samples at 2 K. Inset shows the full range from − 3000 to 3000 Oe; (**d**) $(\chi - \chi_0)^{-1}$ versus temperature plots with temperature range from 100 to 200 K, straight lines show the Curie-Weiss fit. (**e**) The Arrot-Noakes plots measured with magnetic field H from 1 to 5 T and the linear-fitting in high field region for $(Ba_{0.9}Sr_{0.1})(Zn_{0.96}Co_{0.04})_2As_2$.

offers a good example for further experimental,computational and theoretic investigations about the mechanism of the ferromagnetic ordering in bulk form diluted magnetic semiconductors.

| Doping level $x$ | $T_{dif}$ (K) | $\theta$ (K) | $T_C$ (K) | $\mu_{eff}$ ($\mu_B$/Mn) |
|---|---|---|---|---|
| Sb-doped 0.10 | 5 | 32 | – | 1.3 |
| Sb-doped 0.05 | 9 | 42 | – | 1.4 |
| $Ba(Zn_{0.96}Co_{0.04})_2As_2$[28] | 31 | 57 | 45 | 1.4 |
| Sr-doped 0.05 | 33 | 59 | 49 | 1.4 |
| Sr-doped 0.10 | 35 | 62 | 52 | 1.4 |
| Sr-doped 0.15 | 35 | 63 | 53 | 1.4 |

**Table 1.** $T_{dif}$ from the minimum value of dM/dT, Weiss temperature $\theta$ from Curie-Weiss fit, Curie temperature $T_C$ from Arrot-Noakes plots and the effective moment $\mu_{eff}$ for different doping levels $x$.

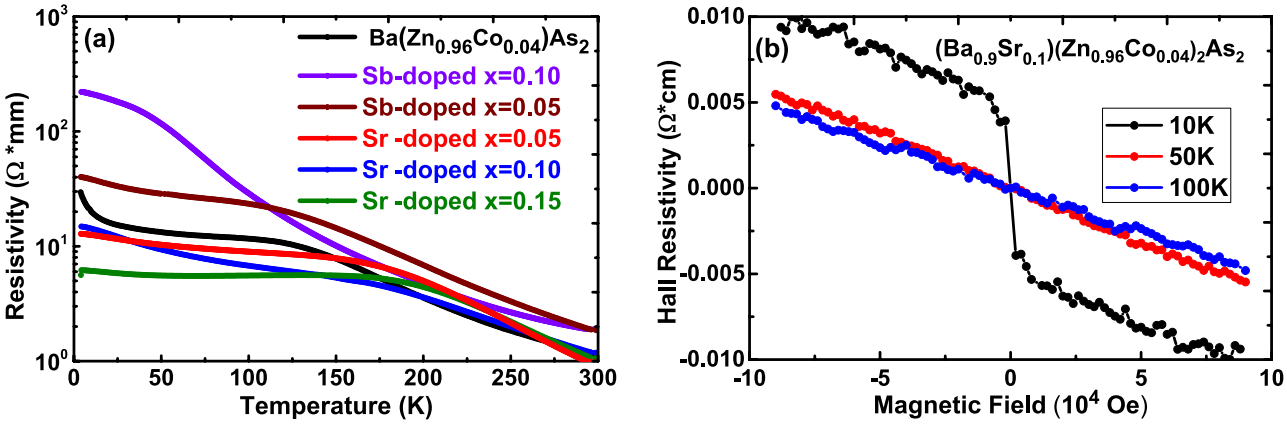


**Figure 3.** (**a**) Temperature-dependent resistivity of $Ba(Zn_{0.96}Co_{0.04})_2As_2$ (extracted from Fig. 5 of ref[28]), Sr-doped and Sb-doped samples. (**b**) Hall resistivity of $(Ba_{0.9}Sr_{0.1})(Zn_{0.96}Co_{0.04})_2As_2$ at different temperatures, demonstrating $n$-type carriers.

## Methods

**Material synthesis.** Polycrystalline samples Sr-doped $(Ba_{1-x}Sr_x)(Zn_{0.96}Co_{0.04})_2As_2$ ($x$ = 0.05, 0.10 and 0.15) and Sb-doped $Ba(Zn_{0.96}Co_{0.04})_2(As_{1-x}Sb_x)_2$ ($x$ = 0.05 and 0.10) were prepared by conventional solid-state reaction method, similarly to that of $Ba(Zn,Co)_2As_2$[28]. High purity Ba, Sr, Zn, Co, As, Sb elements were mixed and placed in alumina crucibles and sealed in evacuated silica tubes. The mixture was heated at 1150 °C for 25 h before cooling to room temperature. The products were then grounded, pressed into pellets, sealed in evacuated silica tubes again and reheated at 1150 °C for another 25 h for further reaction. Then they were quickly cooled to room temperature, the high-temperature phase, tetragonal $\beta$-$BaZn_2As_2$[40] can be obtained.

**Experimental characterization.** The crystal structure of the polycrystalline samples were measured at room temperature using a PANalytical powder X-ray diffractometer with monochromatic Cu-$K_{\alpha 1}$ radiation. The DC magnetization measurements were conducted on a Quantum Design Magnetic Property Measurement System (MPMS). The Hall effect were measured using a Quantum Design Physical Property Measurement System(PPMS). The electrical resistivity was measured on sintered pellets using the typical four-probe method.

## Data availability

All data generated or analysed during this study are included in this published article or available from the corresponding author on reasonable request.

Received: 4 January 2021; Accepted: 3 March 2021
Published online: 07 April 2021

## References

1. Žutić, I., Fabian, J. & Sarma, S. D. Spintronics: Fundamentals and applications. *Rev. Mod. Phys.* **76**, 323–410 (2004).
2. Dietl, T. & Ohno, H. Dilute ferromagnetic semiconductors: Physics and spintronic structures. *Rev. Mod. Phys.* **86**, 187–251 (2014).
3. Dietl, T. A ten-year perspective on dilute magnetic semiconductors and oxides. *Nat. Mater.* **9**, 965–974 (2010).
4. Ohno, H. Making nonmagnetic semiconductors ferromagnetic. *Science* **281**, 951–956 (1998).
5. Ohno, H. *et al.* (Ga, Mn)As: A new diluted magnetic semiconductor based on GaAs. *Appl. Phys. Lett.* **69**, 363–365 (1996).
6. Munekata, H. *et al.* Diluted magnetic III-V semiconductors. *Phys. Rev. Lett.* **63**, 1849–1852 (1989).
7. Sawicki, M. *et al.* Experimental probing of the interplay between ferromagnetism and localization in (Ga, Mn)As. *Nat. Phys.* **6**, 22–25 (2010).
8. Chiba, D., Yamanouchi, M., Matsukura, F. & Ohno, H. Electrical manipulation of magnetization reversal in a ferromagnetic semiconductor. *Science* **301**, 943–945 (2003).

9. Chiba, D., Akiba, N., Matsukura, F., Ohno, Y. & Ohno, H. Magnetoresistance effect and interlayer coupling of (Ga, Mn)As trilayer structures. *Appl. Phys. Lett.* **77**, 1873–1875 (2000).
10. Chen, L. *et al.* Enhancing the Curie temperature of ferromagnetic semiconductor (Ga, Mn)As to 200K via nanostructure engineering. *Nano. Lett.* **11**, 2584–2589 (2011).
11. Hai, P. N. *et al.* Growth and characterization of n-type electron-induced ferromagnetic semiconductor (In, Fe)As. *Appl. Phys. Lett.* **101**, 182403 (2012).
12. Kaneta, S., Anh, L. D., Sriharsha, K. & Tanaka, M. Observation of quantum size effect at the conduction band bottom of n-type ferromagnetic semiconductor (In, Fe)As thin films. *Appl. Phys. Express* **12**, 073001 (2019).
13. Tu, N. T., Hai, P. N., Anh, L. D. & Tanaka, M. Electrical control of ferromagnetism in the n-type ferromagnetic semiconductor (In, Fe)Sb with high curie temperature. *Appl. Phys. Lett.* **112**, 122409 (2018).
14. Deng, Z. *et al.* Li(Zn, Mn)As as a new generation ferromagnet based on a I-II-V semiconductor. *Nat. Commun.* **2**, 1–5 (2011).
15. Deng, Z. *et al.* Diluted ferromagnetic semiconductor Li(Zn, Mn)P with decoupled charge and spin doping. *Phys. Rev. B* **88**, 081203 (2013).
16. Ding, C. *et al.* $(La_{1-x}Ba_x)(Zn_{1-x}Mn_x)AsO$: A two-dimensional 1111-type diluted magnetic semiconductor in bulk form. *Phys. Rev. B* **88**, 041102 (2013).
17. Zhao, K. *et al.* New diluted ferromagnetic semiconductor with curie temperature up to 180K and isostructural to the "122" iron-based superconductors. *Nat. Commun.* **4**, 1–5 (2013).
18. Zhao, K. *et al.* Ferromagnetism at 230K in $(Ba_{0.7}K_{0.3})(Zn_{0.85}Mn_{0.15})_2As_2$ diluted magnetic semiconductor. *Chin. Sci. Bull* **59**, 2524–2527 (2014).
19. Wang, X. C. *et al.* The superconductivity at 18K in LiFeAs system. *Solid State Commun.* **148**, 538–540 (2008).
20. Kamihara, Y., Watanabe, T., Hirano, M. & Hosono, H. Iron-based layered superconductor $La[O_{1-x}F_x]FeAs$(x= 0.05- 0.12) with $T_C$ = 26K. *J. Am. Chem. Soc* **130**, 3296–3297 (2008).
21. Rotter, M., Tegel, M. & Johrendt, D. Superconductivity at 38K in the iron arsenide $(Ba_{1-x}K_x)Fe_2As_2$. *Phys. Rev. Lett.* **101**, 107006 (2008).
22. Ding, C., Qin, C., Man, H., Imai, T. & Ning, F. L. NMR investigation of the diluted magnetic semiconductor $Li(Zn_{1-x}Mn_x)P$ (x= 0.1). *Phys. Rev. B* **88**, 041108 (2013).
23. Guo, S. & Ning, F. Progress of novel diluted ferromagnetic semiconductors with decoupled spin and charge doping: Counterparts of Fe-based superconductors. *Chin. Phys. B* **27**, 097502 (2018).
24. Gu, Y., Guo, S. & Ning, F. Progress on microscopic properties of diluted magnetic semiconductors by NMR and $\mu$SR. *J. Semicond* **40**, 081506 (2019).
25. Peng, Y. *et al.* Effects of chemical pressure on diluted magnetic semiconductor (Ba, K)(Zn, Mn)$_2As_2$. *Chin. Phys. B* **28**, 57501–057501 (2019).
26. Sun, F. *et al.* Pressure effect on the magnetism of the diluted magnetic semiconductor $(Ba_{1-x}K_x)(Zn_{1-y}Mn_y)_2As_2$ with independent spin and charge doping. *Phys. Rev. B* **93**, 224403 (2016).
27. Sun, F. *et al.* Hole doping and pressure effects on the II-II-V-based diluted magnetic semiconductor $(Ba_{1-x}K_x)(Zn_{1-y}Mn_y)_2As_2$. *Phys. Rev. B* **95**, 094412 (2017).
28. Guo, S. *et al.* Ba(Zn, Co)$_2As_2$: A diluted ferromagnetic semiconductor with n-type carriers and isostructural to 122 iron-based superconductors. *Phys. Rev. B* **99**, 155201 (2019).
29. Klüfers, P. & Mewis, A. Zur struktur der verbindungen $BaZn_2P_2$ und $BaZn_2As_2$/The crystal structure of $BaZn_2P_2$ and $BaZn_2As_2$. *Z. Naturforsch. B* **33**, 151–155 (1978).
30. Hellmann, A., Löhken, A., Wurth, A. & Mewis, A. Neue arsenide mit $ThCr_2Si_2$-oder einer damit verwandten struktur: Die verbindungen $ARh_2As_2$ (A: Eu, Sr, Ba) und $BaZn_2As_2$/New arsenides with $ThCr_2Si_2$-type or related structures: The compounds $ARh_2As_2$ (A: Eu, Sr, Ba) and $BaZn_2As_2$. *Z. Naturforsch. B* **62**, 155–161 (2007).
31. Xiao, Z. *et al.* Epitaxial growth and electronic structure of a layered zinc pnictide semiconductor, $\beta$-$BaZn_2As_2$. *Thin Solid Films* **559**, 100–104 (2014).
32. Toby, B. H. & Von Dreele, R. B. GSAS-II: The genesis of a modern open-source all purpose crystallography software package. *J. Appl. Crystallogr.* **46**, 544–549 (2013).
33. Arrott, A. Criterion for ferromagnetism from observations of magnetic isotherms. *Phys. Rev.* **108**, 1394 (1957).
34. Arrott, A. & Noakes, J. E. Approximate equation of state for nickel near its critical temperature. *Phys. Rev. Lett.* **19**, 786 (1967).
35. Yu, S. *et al.* A substantial increase of Curie temperature in a new type of diluted magnetic semiconductors via effects of chemical pressure. *APL Mater.* **7**, 101119 (2019).
36. Beschoten, B. *et al.* Magnetic circular dichroism studies of carrier-induced ferromagnetism in $(Ga_{1-x}Mn_x)As$. *Phys. Rev. Lett.* **83**, 3073–3076 (1999).
37. Glasbrenner, J., Žutić, I. & Mazin, I. Theory of Mn-doped II-II-V semiconductors. *Phys. Rev. B* **90**, 140403 (2014).
38. Dietl, T., Ohno, H. & Matsukura, F. Hole-mediated ferromagnetism in tetrahedrally coordinated semiconductors. *Phys. Rev. B* **63**, 195205 (2001).
39. Keavney, D. J. *et al.* Element resolved spin configuration in ferromagnetic manganese-doped gallium arsenide. *Phys. Rev. Lett.* **91**, 187203 (2003).
40. Xiao, Z. *et al.* Narrow bandgap in $\beta$-$BaZn_2As_2$ and its chemical origins. *J. Am. Chem. Soc.* **136**, 14959–14965 (2014).


## Acknowledgements

The work at Zhejiang was supported by National Basic Research Program of China (No. 2016YFA0300402), NSF of China (No. 12074333), the Key R&D Program of Zhejiang Province, China (2021C01002).

## Author contributions

F.L.N. and L.C.F. conceived this work, L.C.F. conducted the experiments with the help of Y.L.G., H.J.Z., R.F.Z., J.O.D., X.Q.Z. and L.F.X., results were analysed by L.C.F., Y.L.G. and G.X.Z., all authors contributed to the preparation of this manuscript.

## Competing interests

The authors declare no competing interests.

## Additional information

**Correspondence** and requests for materials should be addressed to F.N.

**Reprints and permissions information** is available at www.nature.com/reprints.